Continuation Geometry Resolves Apparent Branch Splitting in Unequal-Mass Three-Body Orbits

Ori Chamo
Incredibuild, Tel Aviv, Israel

Yossi Eliaz*
Incredibuild, Tel Aviv, Israel
islo.dev and
Department of Computer Science, Holon Institute of Technology, Holon, Israel

Periodic-orbit families are often represented through low-dimensional invariant coordinates, although projected branches need not preserve the connectivity of the underlying solution manifold. We use numerical continuation to examine the 135,445 unequal-mass planar three-body periodic orbits reported by Li, Li, and Liao, whose corrected scale-invariant period–angular-momentum representation was subsequently interpreted as two independent sets. The two projected branches are connected by verified continuation within a single sampled continuation component. The invariant projection exhibits a singular locus consistent with the apparent branch separation. High-precision Floquet calculations identify a +1 transition at one representative stability boundary and an opposite-Krein Hamiltonian–Hopf transition at another. Projection geometry and symplectic spectral geometry therefore provide complementary descriptions of the same periodic-orbit manifold.

Periodic orbits organize the dynamics of Hamiltonian systems. As parameters vary, periodic solutions trace continuation manifolds whose geometry and stability changes encode the surrounding dynamics. Such families are commonly displayed through a few scalar observables, including periods, actions, conserved quantities, or scale-invariant combinations [1–3]. These diagrams are projections of the full solution set, so their visible branch structure can differ from continuation connectivity.

Li, Li, and Liao constructed 135,445 unequal-mass non-hierarchical planar periodic orbits on a mass grid at $m_3 = 1$, including 13,315 samples reported as linearly stable [4]. They described the collection as one family. Stančević, Vasiljević, and Dmitrašinović later identified two branches in corrected scale-invariant period–angular-momentum coordinates and interpreted them as independent sets [5]. The resulting dynamical question is whether those projected branches belong to distinct continuation components of the periodic-orbit solution set.

We answer this question by continuing periodic solutions directly through mass and orbit space. We then compute the physical Floquet spectrum after removal of the neutral symmetry directions. Throughout, *continuation component* denotes a connected set of periodic solutions joined by this continuation procedure; stability denotes the nontrivial planar Floquet spectrum of the reduced return map.

The two visible branches of the scale-invariant diagram are joined by verified continuation in both directions within the sampled catalog. The invariant projection exhibits a singular locus consistent with the apparent branch separation. Along the same component, the reduced Floquet spectrum exhibits a +1 transition and an opposite-Krein Hamiltonian–Hopf transition. Three additional mass points satisfy the simultaneous +1 and −1 spectral conditions.

Continuation geometry.—We continue the periodic solutions in the mass parameters (m_1, m_2) at fixed $m_3 = 1$. A periodic solution at one mass point supplies the predictor for a neighboring point, followed by correction of the orbit and period to restore periodicity. Repeating this procedure traces connected branches through the sampled orbit set.

The mass-adjacency graph of the 135,445-point sampled catalog is connected. It contains 270,087 mass-adjacent links and a spanning tree with 135,444 edges. We selected 26 connections that maximize indicators of possible branch separation: five macroscopic graph bottlenecks, the twenty largest chart discontinuities along the spanning tree, and one long-range connection between nearly coincident invariant images. Bidirectional continuation succeeds across all 26 selected connections. The long-range connection was also reproduced in a translation-reduced strict-periodic formulation.

The documented long-range connection joins representative solutions on the two branches of the $(T_{\rm si}, L_{\rm si})$ diagram [Fig. 1]. The visible branch separation therefore occurs within one sampled continuation component.

The corrected scale-invariant period and angular momentum define

$$\Psi(m_1, m_2) = (T_{\rm si}, L_{\rm si}), \tag{1}$$

where $T_{\rm si} = T|E|^{3/2}M^{-5/2}$ and $L_{\rm si} = L|E|^{1/2}M^{-13/6}$, with $M = m_1 + m_2 + m_3$. Centered finite-difference estimates of $D\Psi$ identify a connected locus of adjacent mass cells across which $\det D\Psi$ changes sign. The same audit finds far-separated mass points with nearly coincident invariant coordinates. The discrete record contains 590 determinant-sign-change edges and 86 long-range near coincidences under the stated thresholds.

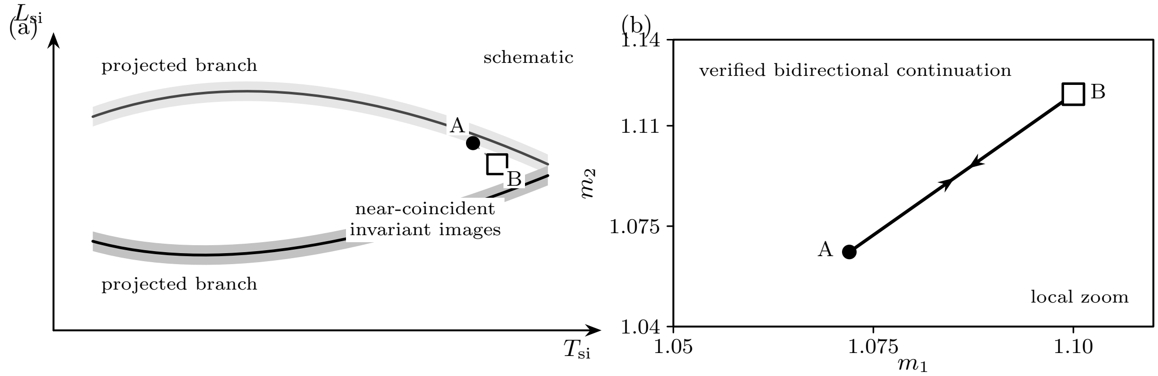

FIG. 1. Continuation connectivity and invariant projection. (a) Schematic of the two branches visible in the corrected scale-invariant period–angular-momentum representation. The documented long-range pair A and B has nearly coincident invariant images. (b) Local zoom of the (m_1, m_2) plane containing the same endpoints. The double-headed segment denotes the continuation verified in both directions. The endpoint mass distance is 0.062. The verified connection links representative points on the two projected branches within the sampled catalog.

These features are consistent with projection geometry underlying the apparent branch separation.

Floquet stability.—After the neutral symmetry directions are removed, each periodic orbit has four nontrivial Floquet multipliers forming two reciprocal pairs. Let $M_{\rm ph}$ be the corresponding 4×4 symplectic return map and define

$$a = \operatorname{tr} M_{\rm ph}, \qquad b = \frac{(\operatorname{tr} M_{\rm ph})^2 - \operatorname{tr}(M_{\rm ph}^2)}{2}. \tag{2}$$

Its characteristic polynomial is

$$\chi(\lambda) = \lambda^4 - a\lambda^3 + b\lambda^2 - a\lambda + 1. \tag{3}$$

With $t = \lambda + \lambda^{-1}$, the two reciprocal pairs are determined by

$$P(t) = t^2 - at + b - 2. \tag{4}$$

Spectral stability requires both roots of P to lie in $[-2, 2]$. The three boundaries are

$$G_+ = P(2) = b - 2a + 2, \tag{5}$$
$$G_- = P(-2) = b + 2a + 2, \tag{6}$$
$$\Delta = a^2 - 4b + 8. \tag{7}$$

The conditions $G_+ = 0$ and $G_- = 0$ place a multiplier at $+1$ and -1, respectively; $\Delta = 0$ marks a collision of the two reciprocal mode traces. The critical curves in mass space are preimages of these boundaries under $\Phi(m_1, m_2) = (a, b)$ [6–8].

Symplecticity pairs each nontrivial multiplier λ with λ^{-1}. For an elliptic multiplier on the unit circle, the Krein signature is the sign of its associated symplectic quadratic form.

Stability transitions.—Along $m_1 = 0.8023446$, the lower representative stability boundary occurs near $m_2 = 0.75401872$. On the unstable side, the relevant Floquet modes form a real reciprocal pair. Approaching the boundary, the pair reaches $+1$; beyond the boundary it lies on the unit circle [Fig. 2(b)]. An independent 60-digit implementation reproduces the transition within an m_2 bracket of width 1.6×10^{-9}.

Along $m_1 = 0.8022890$, two elliptic Floquet modes approach one another on the unit circle at the upper representative stability boundary. Their Krein signatures have opposite signs on the stable side. At the boundary the modes collide, and beyond it the spectrum forms a reciprocal complex quartet off the unit circle [Fig. 2(c)]. This is an opposite-Krein Hamiltonian–Hopf transition. The independent 60-digit calculation reproduces the critical location within an m_2 bracket of width 6.3×10^{-9}.

The $+1$ and -1 boundaries meet at the physical spectral vertex $(a, b) = (0, -2)$. Solving $G_+ = G_- = 0$ yields three mixed spectral intersections in the sampled mass domain. Their coordinates and residuals are listed in the Supplemental Material. All three were recomputed at 60-digit precision.

Direct continuation thus connects the two projected branches within one sampled component of the LLL periodic-orbit manifold. The numerically resolved singular locus is consistent with their apparent separation in the invariant projection. The reduced Floquet spectrum distinguishes a $+1$ transition from an opposite-Krein Hamiltonian–Hopf transition along that component, while three additional mass points map to the mixed $+1/-1$ spectral vertex. Projected branch structure and continuation connectivity therefore encode different information. The same distinction applies whenever a multidimensional periodic-orbit family is classified through a small number of projected invariants.

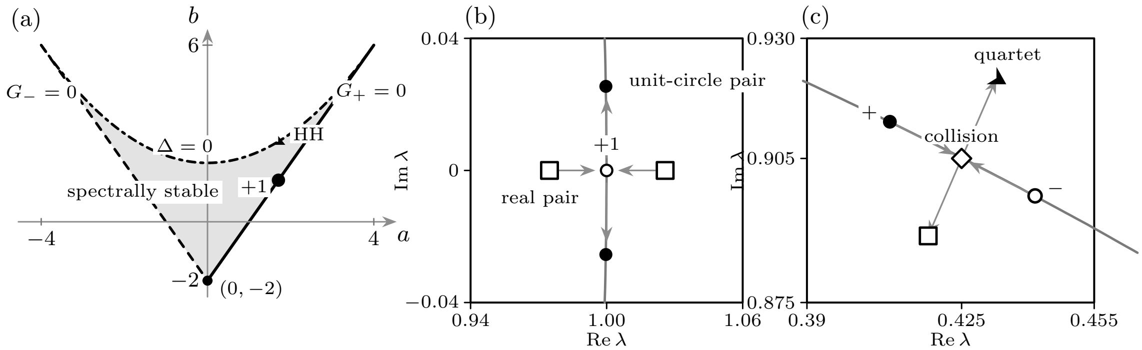

FIG. 2. Distinct Floquet mechanisms on the continuation component. (a) Stability geometry in the physical Sp(4) trace plane. The boundaries $G_+ = 0$ (solid), $G_- = 0$ (dashed), and $\Delta = 0$ (dot-dashed) correspond to $+1$, -1, and mode-collision conditions. The filled circle marks the lower $+1$ transition and the filled triangle the upper Hamiltonian–Hopf transition; the mixed vertex is $(a, b) = (0, -2)$. (b) A real reciprocal pair (open squares) reaches $+1$ and becomes an elliptic unit-circle pair (filled circles). (c) Two unit-circle modes of opposite Krein signature (filled $+$ and open $-$) converge to the collision point. Beyond the collision, the upper-half representatives move to opposite sides of the unit circle; their conjugates complete a reciprocal complex quartet.

END MATTER

Numerical continuation. Planar Newtonian motion is integrated with $G = 1$ at fixed $m_3 = 1$. The published collinear shooting chart has unknowns (x_1, v_1, v_2, T), with total momentum removed. A neighboring sample supplies the predictor and a Newton corrector restores periodicity in center-of-mass-reduced coordinates. The long-range connection joins $(m_1, m_2) = (1.072, 1.066)$ and $(1.100, 1.121)$. Bidirectional continuation gives shooting residual below 2.3×10^{-10} and terminal chart mismatch below 6×10^{-13}.

Physical Floquet calculation. The variational equation is integrated in canonical Jacobi coordinates. The Hamiltonian and angular-momentum symmetry directions are removed through the physical quotient E^{ω}/E, leaving M_{ph}. The eight-dimensional trace convention used in parts of the numerical archive is related by $\alpha = a + 4$ and $\beta = b + 4a + 6$; hence the physical mixed vertex $(0, -2)$ is $(4, 4)$ in that convention.

High-precision verification. An independent implementation uses 60-digit arithmetic, a ninth-order Verner integrator, canonical Jacobi variational equations, and the physical quotient. The two transitions have sign-changing brackets in m_2, closure norms of order 10^{-21}–10^{-22}, and symplectic defects of order 10^{-19}–10^{-20}. The mixed-root event residuals range from 10^{-14} to 10^{-13}.

OpenAI ChatGPT (GPT-5.6 Pro) and xAI Grok 4.6 assisted with manuscript editing, figure layout, and software review. The authors checked the resulting changes against the source code and numerical records and take responsibility for the manuscript and conclusions.

Data availability. Data and code are available in Ref. [9]; the source orbit catalog is Ref. [4].

* eliazy@hit.ac.il

[1] A. Chenciner and R. Montgomery, A remarkable periodic solution of the three-body problem in the case of equal masses, Annals of Mathematics 2, **152**, 881 (2000), arXiv:math/0011268.

[2] J. Galán, F. J. Muñoz-Almaraz, E. Freire, E. Doedel, and A. Vanderbauwhede, Stability and bifurcations of the figure-8 solution of the three-body problem, Physical Review Letters **88**, 241101 (2002).

[3] X. Li and S. Liao, A review on periodic orbits of the general planar three-body problem, Science China Physics, Mechanics & Astronomy **68**, 289501 (2025).

[4] X. Li, X. Li, and S. Liao, One family of 13315 stable periodic orbits of the non-hierarchical unequal-mass triple system, Science China Physics, Mechanics & Astronomy **64**, 219511 (2021), arXiv:2007.10184 [nlin.CD].

[5] D. Stančević, V. Vasiljević, and V. Dmitrašinović, The mass-, period- and angular momentum dependences of the "moth-i" family of 3-body orbits, SSRN preprint (2023).

[6] V. A. Yakubovich and V. M. Starzhinskii, *Linear Differential Equations with Periodic Coefficients* (Wiley, New York, 1975).

[7] J. E. Howard and R. S. MacKay, Linear stability of symplectic maps, Journal of Mathematical Physics **28**, 1036 (1987).

[8] U. Frauenfelder, D. Koh, and A. Moreno, Symplectic methods in the numerical search of orbits in real-life planetary systems, SIAM Journal on Applied Dynamical Systems **22**, 3284 (2023).

[9] O. Chamo and Y. Eliaz, Continuation geometry of unequal-mass three-body periodic orbits: numerical records and source code, GitHub repository (2026).

Supplemental Material for Continuation Geometry Resolves Apparent Branch Splitting in Unequal-Mass Three-Body Orbits

Ori Chamo
Incredibuild, Tel Aviv, Israel

Yossi Eliaz*
Incredibuild, Tel Aviv, Israel
islo.dev and
Department of Computer Science, Holon Institute of Technology, Holon, Israel

This Supplemental Material records the catalog conventions, continuation tests, invariant-projection audit, Floquet reduction, high-precision transition data, mixed intersections, and the broader numerical survey supporting the Letter. All numerical values are taken from the existing committed records; no new orbit integrations are introduced here.

CATALOG, NORMALIZATION, AND TERMINOLOGY

The Li–Li–Liao table contains 135,445 non-hierarchical unequal-mass planar periodic-orbit samples on $m_1 \in [0.8, 1.1]$, $m_2 \in [0.7, 1.2]$, $m_3 = 1$, with mass spacing 0.001. The source reports 13,315 samples as linearly stable [1]. The numerical archive accepts the upstream bytes only when their Git blob is `79b2963df43e62201c35690bfc22bec166132427`.

The scale-invariant coordinates used in the projection analysis are

$$T_{\mathrm{si}} = T|E|^{3/2} M^{-5/2}, \qquad L_{\mathrm{si}} = L|E|^{1/2} M^{-13/6}, \tag{1}$$

where $M = m_1 + m_2 + m_3$. The corresponding map is $\Psi(m_1, m_2) = (T_{\mathrm{si}}, L_{\mathrm{si}})$.

Every catalog entry carries the same reported syzygy word $bABabaBAba$. Topological-word conventions follow the standard shape-sphere construction [2, 3]. The present component classification is determined by continuation of periodic solutions.

CONTINUATION AND BRANCH MATCHING

The published samples use the collinear shooting chart

$$\begin{aligned} \mathbf{r}_1 &= (x_1, 0), \qquad \mathbf{r}_2 = (1, 0), \qquad \mathbf{r}_3 = (0, 0), \\ \mathbf{v}_1 &= (0, v_1), \qquad \mathbf{v}_2 = (0, v_2), \end{aligned} \tag{2}$$

with $\mathbf{v}_3$ fixed by zero total momentum. At fixed masses, the shooting unknowns are (x_1, v_1, v_2, T). A neighboring solution supplies the predictor; a Newton correction in center-of-mass-reduced coordinates restores periodicity. A connection is accepted when the continuation converges in both directions and the terminal shooting coordinates match the independently corrected endpoint.

The 135,445 samples form a connected mass-adjacency graph with 270,087 adjacent links and a spanning tree containing 135,444 edges. Twenty-six connections were selected to maximize indicators of possible separation: five macroscopic bottlenecks, the twenty largest chart discontinuities along the spanning tree, and one long-range pair with nearly coincident invariant images. Bidirectional continuation succeeds for all 26.

The long-range pair is

$$(m_1, m_2)_A = (1.072, 1.066), \qquad (m_1, m_2)_B = (1.100, 1.121), \tag{3}$$

with Euclidean mass distance 0.0617. Eighty continuation steps in each direction give maximum shooting residual below 2.3×10^{-10} and terminal normalized chart mismatch below 6×10^{-13}. The same endpoints were also connected in a translation-reduced strict-periodic formulation outside the published collinear-velocity ansatz.

INVARIANT-PROJECTION AUDIT

Centered finite differences of Ψ on the published grid produce 134,046 interior Jacobian estimates. Their normalized determinants have both signs: 113,514 positive and 20,532 negative. There are 590 adjacent determinant-sign-change edges, whose incident nodes form one connected locus in the sampled mass plane. The minimum normalized singular-value ratio is approximately 1.39×10^{-6}.

A nearest-neighbor search in standardized $(T_{\mathrm{si}}, L_{\mathrm{si}})$ coordinates also identifies distant masses with nearly coincident invariant images. Among rows whose selected invariant neighbor is at least 0.05 away in mass, 86 pairs have standardized invariant distance below 10^{-4}. The long-range continuation pair above is one of these near coincidences. These statistics describe a discrete singularity and non-unique appearance of the sampled projection; the continuation test supplies the dynamical connection.

PHYSICAL FLOQUET REDUCTION

The variational equations are integrated in canonical Jacobi coordinates. The Hamiltonian and angular-momentum neutral directions span $E = \mathrm{span}\{X_H, X_L\}$ and are removed through the quotient E^ω/E. The resulting physical return map M_{ph} is a 4×4 symplectic matrix. Define

$$a = \mathrm{tr}\, M_{\mathrm{ph}}, \qquad b = \frac{(\mathrm{tr}\, M_{\mathrm{ph}})^2 - \mathrm{tr}(M_{\mathrm{ph}}^2)}{2}. \tag{4}$$

Then

$$\chi(\lambda) = \lambda^4 - a\lambda^3 + b\lambda^2 - a\lambda + 1 \tag{5}$$

and, for $t = \lambda + \lambda^{-1}$,

$$P(t) = t^2 - at + b - 2. \tag{6}$$

The physical critical functions are

$$G_+ = b - 2a + 2, \qquad G_- = b + 2a + 2, \qquad \Delta = a^2 - 4b + 8. \tag{7}$$

The physical spectral vertices are $(-4, 6)$ (double -1), $(0, -2)$ (mixed $+1/-1$), and $(4, 6)$ (double $+1$).

Some archived screening records use invariants derived from the unreduced 8×8 monodromy. They are related to the physical invariants by

$$\alpha = a + 4, \qquad \beta = b + 4a + 6. \tag{8}$$

Thus the three physical vertices map to $(0, -4)$, $(4, 4)$, and $(8, 28)$ in the archive convention. The mechanism labels and mass coordinates are unchanged by this affine change of coordinates.

HIGH-PRECISION PLUS-ONE TRANSITION

At $m_1 = 0.8023446113666945$, an independent 60-digit implementation encloses the lower transition in

$$0.7540187211922449 \le m_2 \le 0.7540187227698909, \tag{9}$$

with bracket width 1.577646×10^{-9} and a sign change of G_+. On the smaller-m_2 flank the relevant physical multipliers form a real reciprocal pair approximately $(0.9748, 1.0258)$. On the larger-m_2 flank the pair is approximately $0.99968 \pm 0.02547i$ on the unit circle. The reduced closures are of order 10^{-21} and the physical symplectic defects are of order 10^{-19}.

HIGH-PRECISION HAMILTONIAN–HOPF TRANSITION

At $m_1 = 0.8022889780964406$, the upper transition lies in

$$0.7592347034247101 \leq m_2 \leq 0.7592347096924873, \tag{10}$$

with bracket width 6.267777×10^{-9} and a sign change of Δ. On the stable flank the upper-half unit modes are $0.40876 + 0.91264i$ and $0.44163 + 0.89720i$. Their Krein forms have opposite signs, approximately $+3.76 \times 10^{-3}$ and -3.72×10^{-3}. On the unstable flank the spectrum is a reciprocal complex quartet with maximum radius deviation 1.83×10^{-2}. The reduced closures are of order 10^{-22} and the physical symplectic defects are of order 10^{-20}.

MIXED PLUS-ONE/MINUS-ONE SPECTRAL INTERSECTIONS

Simultaneous 60-digit Newton solves of $G_+ = G_- = 0$ yield the three mass points in Table I. Each maps to the physical mixed vertex $(a, b) = (0, -2)$, or equivalently $(\alpha, \beta) = (4, 4)$ in the archive convention.

TABLE I. Mixed $+1/-1$ intersections at $m_3 = 1$. The final column is the relative norm of the two event functions in the archived record.

Location	m_1	m_2	Relative event norm
Principal left	0.9292391921	0.8853664625	1.5×10^{-13}
Secondary left	0.9967681995	0.9560193602	1.2×10^{-14}
Principal right	1.0495531867	1.1294758073	3.1×10^{-14}

BROADER CRITICAL SURVEY AND NUMERICAL SENSITIVITY

The published table contains 620 adjacent cells whose reported linear stability label changes. The survey localizes one critical point in each cell: 198 of type G_+, 168 of type G_-, and 254 of type Δ. A full-domain sign sweep contributes additional sampled event curves. This survey is retained as a map of sampled event preimages; it is not used as an exhaustive classification of every critical curve.

Of the 620 published transition cells, 462 retain binary64 localization and 158 have arbitrary-precision corroboration. Equivalent double-precision coordinate formulations move the event value by more than 2×10^{-8} on 345 of the 620 cells. Arbitrary-precision escalation of sixteen difficult cells changed four mechanism labels from G_+ to Δ. These sensitivity results are the reason the two headline transitions are reported from the independent 60-digit calculation.

Two sampled survey ends remain unclassified, near $(0.892, 0.75308)$ and $(1.042, 0.85798)$. They do not affect the continuation-component statement or the two representative high-precision transitions reported in the Letter.

REPRODUCIBILITY

The Python and Julia environments, evidence records, figure sources, and submission sources are available in Ref. [4]. The upstream catalog is cited in Ref. [1] and is not redistributed.

* eliazy@hit.ac.il

[1] X. Li, X. Li, and S. Liao, One family of 13315 stable periodic orbits of the non-hierarchical unequal-mass triple system, Science China Physics, Mechanics & Astronomy **64**, 219511 (2021), arXiv:2007.10184 [nlin.CD].
[2] R. Montgomery, The geometric phase in the three-body problem (1995), arXiv:dg-ga/9510005 [dg-ga].
[3] R. Moeckel and R. Montgomery, Symmetric regularization, reduction and blow-up of the planar three-body problem (2012), arXiv:1202.0972 [math.DS].
[4] O. Chamo and Y. Eliaz, Continuation geometry of unequal-mass three-body periodic orbits: numerical records and source code, GitHub repository (2026).